

This is a postprint version of the following published document:

Reboul, J., et al. Influence of strain rate sensitivity on localization and void coalescence, In: *International journal of plasticity*, 125 (Feb. 2020), Pp. 265-279

DOI: <https://doi.org/10.1016/j.ijplas.2019.09.007>

© 2019 Elsevier Ltd. All rights reserved.



This work is licensed under a [Creative Commons Attribution-NonCommercial-NoDerivatives 4.0 International License](https://creativecommons.org/licenses/by-nc-nd/4.0/).

Influence of Strain Rate Sensitivity on Localization and Void Coalescence

Javier Reboul^a, Ankit Srivastava^b, Shmuel Osovski^c, Guadalupe Vadillo^{a,*}

^a*Department of Continuum Mechanics and Structural Analysis, University Carlos III of Madrid, Avda. de la Universidad, 30, 28911 Leganés, Madrid, Spain*

^b*Department of Materials Science and Engineering, Texas A&M University, College Station, TX, USA*

^c*Faculty of Mechanical Engineering, Technion-Israel Institute of Technology, Haifa, Israel*

Abstract

The onset of macroscopic strain localization limits the ductility of many ductile materials. For porous ductile materials, two distinct mechanisms of macroscopic localization have been identified: void growth induced softening and void coalescence. In this work we focus on analyzing the influence of materials strain rate sensitivity (SRS) on the two mechanisms of macroscopic localization or ductile failure as a function of the imposed stress triaxiality. To this end, three dimensional finite element calculations of unit cells have been carried out to model void growth and coalescence in an infinite block containing a periodic distribution of initially spherical voids in a band. The matrix material of the unit cell is considered to follow a strain rate dependent elastic perfectly plastic flow response. The unit cell calculations are carried out for a range of SRS parameter, imposed stress triaxiality and initial orientations of the voided band. Our results show that both the critical porosity and strain at the onset of localization and coalescence are strongly influenced by the SRS parameter and the imposed stress triaxiality values. Furthermore, the relative effect of the SRS parameter is found to increase with the increasing value of the imposed stress triaxiality.

Keywords: Ductility (A), Fracture Mechanisms (A), Elastic-viscoplastic Material (B), Porous Material (B), Finite Elements (C)

1. Introduction

The ductility of metals and alloys is limited by the onset of macroscopic strain localization, as it marks the end of uniform deformation and acts as a precursor to failure. Two distinct mechanisms have been identified that can lead to macroscopic strain localization in porous ductile materials (Tekoğlu et al., 2015).

The first mechanism of macroscopic strain localization involves strain softening due to microstructural changes, thermal effects and/or damage evolution resulting in local degradation in material's load carrying capacity. The local degradation in the material's load carrying capacity, causes localized deformation in a thin band with smoothly varying deformation pattern outside the

*

Email address: gvadillo@ing.uc3m.es (Guadalupe Vadillo)

10 band (Fressengeas and Molinari, 1985; Tvergaard, 1981; Pardoen and Hutchinson, 2000; Mercier
11 and Molinari, 2003; Aretz, 2007; Pineau et al., 2016). This results in a weak discontinuity along the
12 thin band at the micro-scale and a discontinuity in the displacement field at the macro-scale. In
13 porous ductile materials, damage (void growth) induced softening is the dominant mechanism that
14 triggers the onset of macroscopic localization (Tvergaard, 1982), resulting in void sheet fracture.
15 The width of the thin band engulfing the voids in this scenario has a length scale comparable
16 or greater than the mean spacing between the voids. Under these circumstances the onset of
17 macroscopic localization is strongly dependent on material properties, initial porosity, orientation
18 of the band undergoing localized deformation and the imposed stress state (Needleman and Rice,
19 1978; Yamamoto, 1978).

20 The second mechanism of macroscopic strain localization in porous ductile materials involves
21 void coalescence. Void coalescence is a local instability phenomenon where the interaction between
22 neighboring voids plays a critical role. The onset of void coalescence is associated with a sudden
23 concentration of plastic strain in the ligaments linking neighboring voids (Koplik and Needleman,
24 1988). Thus, following the onset of void coalescence, the kinematics of the void enlargement
25 significantly differs from that of void growth prior to this instability mode. For void coalescence
26 induced macroscopic localization the width of the micro-scale localization band is much more
27 narrower because the deformation is limited to the ligaments between the neighbouring voids.

28 The two aforementioned mechanisms of macroscopic localization in porous ductile materials,
29 void growth induced softening and void coalescence, are distinct and have been identified in
30 Tekoğlu et al. (2015); Guo and Wong (2018). In particular, for a strain rate independent material,
31 Tekoğlu et al. (2015) showed that depending on the value of the imposed stress triaxiality a
32 clear separation exists between the two mechanisms of macroscopic localization. This raises a
33 fundamental question: how does the material's strain rate sensitivity affect the two mechanisms
34 of macroscopic localization or ductile failure as a function of the imposed stress triaxiality?

35 The strain rate sensitivity is an important material parameter and it greatly affects the onset of
36 localized deformation and damage evolution (Marciniak et al., 1973; Hutchinson and Neale, 1977;
37 Ghosh, 1977; Hutchinson et al., 1978; Taya and Seidel, 1981; Budiansky et al., 1982; Cocks and
38 Ashby, 1982a,b; Pan, 1983a; Pan et al., 1983; Yoon and Taya, 1984; Duva, 1986; Nemat-Nasser
39 et al., 1986; Ortiz and Molinari, 1992; Czarnota et al., 2006; Vadillo et al., 2012; Srivastava and
40 Needleman, 2013; Agoras and Ponte Castañeda, 2014; Osovski et al., 2015; Wang et al., 2018). This
41 in turn affects the performance, safety, reliability and manufacturability of engineering components
42 and structures; for example, the crash worthiness of automobiles, the blast resistance of ships and
43 airplane cargo holds, and the manufacturability of sheet metal components. In general, increasing
44 the strain rate sensitivity of a ductile material can delay the onset of localized plastic deformation.
45 Furthermore, it has also been shown that an increase in the material's strain rate sensitivity can
46 slow down the evolution of porosity and delay the onset of void coalescence in a porous ductile
47 material. In this work we focus on analyzing the influence of materials strain rate sensitivity on
48 the two mechanisms of macroscopic localization or ductile failure as a function of the imposed
49 stress triaxiality.

50 Several analytical and computational studies have been carried out in past to analyze the
51 onset of localized deformation (Marciniak and Kuczyński, 1967; Rudnicki and Rice, 1975; Rice,
52 1977; Saje et al., 1982; Pan, 1983b; Mear and Hutchinson, 1985; Nahshon and Hutchinson, 2008).
53 The micro-mechanical approach that constitute the basis of these works involves analyzing an

54 infinite sheet or block with a defect band inclined at an angle with respect to the imposed loading
55 direction. Alternatively, the onset of localization in a porous material can also be analyzed via unit
56 cell model calculations. In the unit cell model calculations, a periodic distribution of voids in the
57 material is assumed, that allows us to model a single void in the material and impose proportional
58 loading throughout the deformation history (Koplik and Needleman, 1988; Scheyvaerts et al., 2011;
59 Fritzen et al., 2012; Srivastava and Needleman, 2013; Brünig et al., 2013; Dunand and Mohr, 2014;
60 Tekoğlu et al., 2015; Liu et al., 2016; Torki et al., 2017; Guo and Wong, 2018; Luo and Gao, 2018).
61 Thus, unit cell model calculations not only provide the macroscopic response of the material but
62 also provide the details of the void growth and coalescence, as a function of the imposed constant
63 stress triaxiality values.

64 In this work, three dimensional finite element calculations of unit cells have been carried out
65 to model macroscopic strain localization due to damage induced softening, void growth and/or
66 coalescence, in an infinite block containing a periodic distribution of initially spherical voids in
67 a band. *Note that we have assumed a state of the material where either the voids are initially
68 present or have already nucleated (uniformly for the sake of simplicity) in a narrow region in the
69 material.* The unit cell modeled consists of a central block with a single void in its center within
70 two semi-infinite void-free blocks. *The matrix material of the unit cell is considered to follow a
71 strain rate dependent elastic perfectly plastic flow response. Limited calculations have also been
72 carried out to explore the combined effect of material’s strain rate sensitivity and strain hardening.
73 The unit cell calculations are carried out for one initial void volume fraction, a range of strain rate
74 sensitivity parameter, a range of imposed stress triaxiality, and three initial orientations of the
75 voided band. In the calculations, onset of macroscopic localization is defined as the point when
76 the ratio of the rate of deformation in the band and outside the band reaches a critical level, while
77 the onset of void coalescence is defined when the ratio of the maximum to the minimum effective
78 plastic strain rate at the surface of the void reaches a critical value following the work of Tekoğlu
79 et al. (2015); Guo and Wong (2018).*

80 The remainder of this paper are organized as follows. The problem formulation and numerical
81 method are detailed in Section 2. The numerical results and the discussion of the key results are
82 presented in Section 3. The main conclusions of this work are summarized in Section 4.

83 2. Problem Formulation and Numerical Method

84 Three dimensional finite element calculations are carried out to model plastic flow localization
85 and void coalescence in an infinite block containing a periodic distribution of initially spherical
86 voids in a band as shown in Fig. 1 (top left). The configuration analyzed here is numerically
87 similar to the works of Tvergaard (1989); Barsoum and Faleskog (2011); Tekoğlu et al. (2015) and
88 Guo and Wong (2018).

89 2.1. Unit Cell Model

90 As shown in Fig. 1, for the periodic distribution of the voids in the voided band, a unit cell
91 can be defined as a central block with a single void in its center within two void-free semi-infinite
92 blocks. The initial volume of the central block is taken to be $V_{central\ block} = D_{10}D_{20}D_{30} = D_0^3$
93 and the initial volume fraction of the spherical void with radius R_0 is $f_0 = 4\pi R_0^3/3D_0^3$. In the
94 finite element calculations, the semi-infinite blocks along x_1 direction are assumed to be of finite

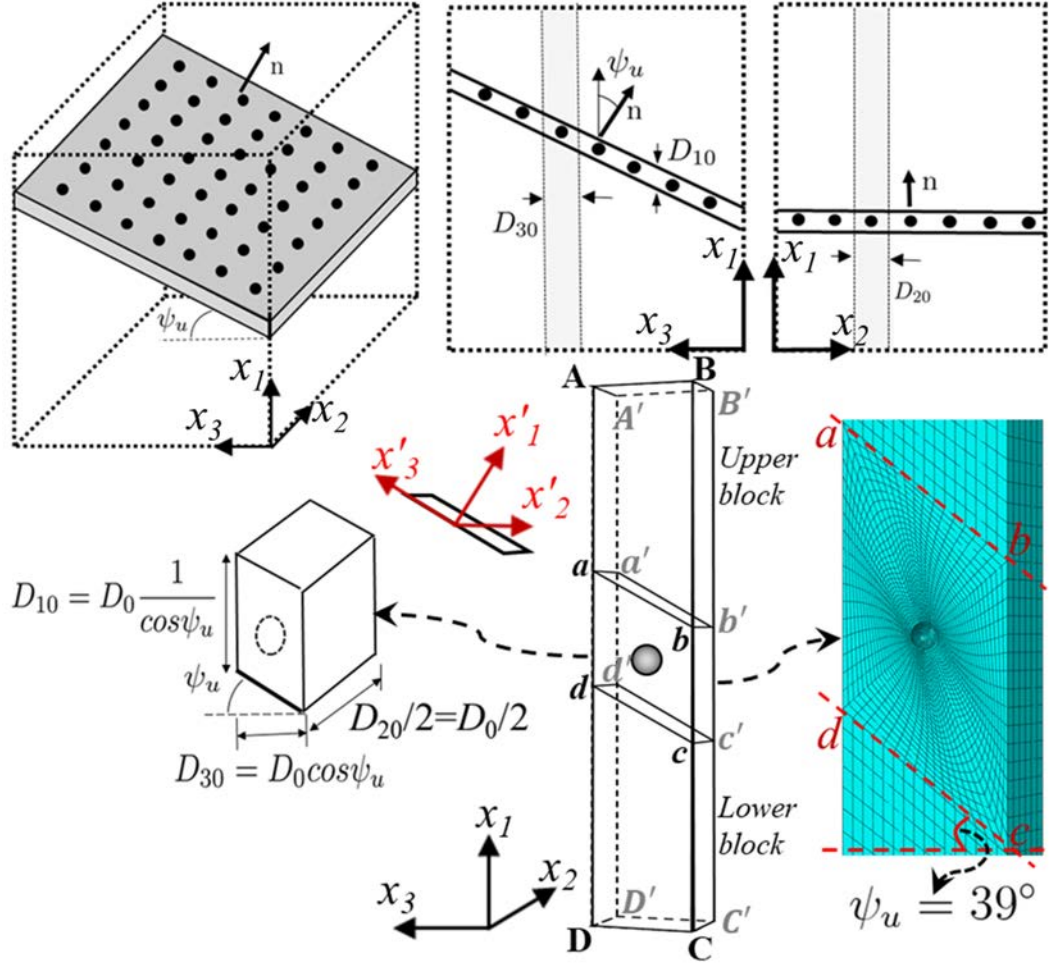


Figure 1: Three dimensional representation of an infinite block containing a periodic distribution of initially spherical voids in a band initially inclined at an angle ψ_u with respect to the x_2 - x_3 plane (top left). The two dimensional sections of the block along x_1 - x_3 (top center) and x_1 - x_2 (top right) planes are also shown in the figure to highlight the periodicity of the voids. Owing to the periodic distribution of the voids, the voided band can be represented as a central block with a single void in its center within two void-free semi-infinite blocks (bottom center). The initial dimensions of the central block are D_{10} , D_{20} , and D_{30} along x_1 , x_2 and x_3 axes, respectively (bottom left). A zoomed in view of the finite element model of 1/2 unit cell with initial void volume fraction, $f_0 = 0.001$ and $\psi_u = 39^\circ$ (bottom right).

95 length but long enough to numerically mimic semi-infinite blocks. For a given loading state and
 96 orientation angle, ψ_u , of the voided band in the initial state, the orientation angle of the band at
 97 any deformation angle ψ progress with the deformation of the outer blocks as:

$$\tan(\psi) = e^{(E_1 - E_3)} \tan(\psi_u) \quad (1)$$

$$\dot{\psi} = \frac{1}{2} \sin(2\psi) (\dot{E}_1 - \dot{E}_3) \quad (2)$$

98 where, E_1 , E_2 , E_3 , are the macroscopic logarithmic principal strains given as:

$$E_1 = \ln(\lambda_1), \quad E_2 = \ln(\lambda_2), \quad E_3 = \ln(\lambda_3) \quad (3)$$

99 In Eq. (3), $\lambda_1 = L_1/L_{10}$, $\lambda_2 = L_2/L_{20}$ and $\lambda_3 = L_3/L_{30}$, with L_{i0} being the initial, and L_i
 100 being the current lengths of the unit cell along x_i axes. The current lengths of the unit cell follow,

$$L_1 = L_{10} + U_1; \quad L_2/2 = L_{20}/2 + U_2; \quad L_3 = L_{30} + U_3 \quad (4)$$

101 where, U_i , are taken at point A' in Fig. 1. Following Eq. (3), the rates of macroscopic loga-
 102 rithmic principal strains are:

$$\dot{E}_1 = \frac{\dot{\lambda}_1}{\lambda_1}, \quad \dot{E}_2 = \frac{\dot{\lambda}_2}{\lambda_2}, \quad \dot{E}_3 = \frac{\dot{\lambda}_3}{\lambda_3} \quad (5)$$

103 The unit cell shown in Fig. 1 (bottom) is symmetric along x_2 axis, so that only 1/2 of the unit
 104 cell needs to be analyzed. The boundary conditions $u_2^{ABba} = u_2^{abcd} = u_2^{dcCD} = 0$ and $u_2^{A'B'b'a'} =$
 105 $u_2^{a'b'c'd'} = u_2^{d'c'C'D'} = U_2$ are imposed on the external faces of the unit cell normal to x_2 axis. Also,
 106 we assume that the external faces of the upper and lower blocks of the unit cell (see Fig. 1) that
 107 are initially straight and normal to the x_1 and x_3 axes remain normal and straight throughout
 108 the deformation history. This results in boundary conditions, $u_1^{DD'C'C} = 0$ and $u_1^{AA'B'B} = U_1$, and
 109 $u_3^{BB'b'b} = u_3^{c'C'C} = 0$ and $u_3^{AA'a'a} = u_3^{d'D'D} = U_3$. Next, following Tvergaard (1989), boundary
 110 conditions applied on the external faces of the band in the unit cell that are initially straight and
 111 normal to the x_3 axis are,

$$\begin{aligned} u_1^{aa'd'd} - u_1^{bb'c'c} &= L_{30} (e^{E_3} \tan(\psi) - \tan(\psi_u)) \\ u_3^{aa'd'd} - u_3^{bb'c'c} &= L_{30} (e^{E_3} - 1) \end{aligned} \quad (6)$$

112 where, $L_{30} = D_{30} = D_0 \cos(\psi_u)$.

113 The voided part of the cell is weaker than the outer blocks. This is reflected by additional
 114 rigid body displacements among the outer blocks with values $2\Delta_1$ and $2\Delta_3$. The values Δ_1 and
 115 Δ_3 vanish if the cell has no void. By symmetry, there is no relative displacement of the outer
 116 blocks in x_2 direction. The corresponding relative displacement field in the upper block outside
 117 the voided cell (evaluated at point a in Fig. 1 and relative to the center of the void) can then be
 118 given as:

$$\begin{aligned} u_1 &= (\lambda_1 - 1) x_1 + \Delta_1 \\ u_2 &= (\lambda_2 - 1) x_2 \\ u_3 &= (\lambda_3 - 1) x_3 + \Delta_3 \end{aligned} \quad (7)$$

119 The strain rate components in the band, \dot{E}_{ij}^b , are the result of the sum of the uniform strain
 120 outside the band plus the strain associated with the rigid body displacements Δ_1 and Δ_3 :

$$\dot{E}_{11}^b = \cos^2(\psi) \dot{E}_1 + \sin^2(\psi) \dot{E}_3 + \frac{2\dot{\Delta}_1 \cos(\psi) - 2\dot{\Delta}_3 \sin(\psi)}{H}$$

$$\begin{aligned}
\dot{E}_{22}^b &= \dot{E}_2 \\
\dot{E}_{33}^b &= \sin^2(\psi) \dot{E}_1 + \cos^2(\psi) \dot{E}_3 \\
\dot{E}_{13}^b &= \sin(2\psi) (\dot{E}_1 - \dot{E}_3) + \frac{2\dot{\Delta}_3 \cos(\psi) + 2\dot{\Delta}_1 \sin(\psi)}{H}
\end{aligned} \tag{8}$$

121 Here, the components of \dot{E}_{ij}^b are defined with respect to the local axes (x'_1, x'_2, x'_3) attached
122 to the band that consequently rotates with the band.

123 The components of the strain rate \dot{E}_{ij} are however expressed with respect to x_1, x_2 and x_3 axes.
124 H is the current thickness of the band (in x'_1 direction), being $H_0 = D_{10} \cos \psi_u$, with $\dot{H} = \dot{E}_{11}^b H$.

125 The \dot{E}_{eq}^b and \dot{E}_{eq} are given as:

$$\dot{E}_{eq}^b = \sqrt{\frac{2}{3} \dot{E}_{ij}^b \dot{E}_{ij}^b}, \quad \dot{E}_{eq} = \sqrt{\frac{2}{3} (\dot{E}_1^2 + \dot{E}_2^2 + \dot{E}_3^2)} \tag{9}$$

126 and, $E_{eq}^b = \int_0^t \dot{E}_{eq}^b d\tau$ and $E_{eq} = \int_0^t \dot{E}_{eq} d\tau$.

127 The macroscopic true principal stresses Σ_1, Σ_2 and Σ_3 , or the average reaction forces per unit
128 area at the deformed cell boundary, are defined in terms of the Cauchy stress components, σ_{ii} , as:

$$\Sigma_i = \frac{1}{L_j L_k} \int_0^{L_j} \int_0^{L_k} [\sigma_{ii}]_{x_i=L_i} dx_j dx_k \quad \text{with } i, j, k = 1, 2, 3$$

129 The macroscopic stress triaxiality, T , and the Lode parameter, L are defined as:

$$T = \frac{\Sigma_h}{\Sigma_{eq}}; \quad L = \frac{2\Sigma_2 - \Sigma_1 - \Sigma_3}{\Sigma_1 - \Sigma_3} \tag{10}$$

130 with Σ_h and Σ_e being the hydrostatic and equivalent macroscopic stresses, respectively, and
131 are given as:

$$\Sigma_h = \frac{\Sigma_1 + \Sigma_2 + \Sigma_3}{3}, \quad \Sigma_{eq} = \frac{1}{\sqrt{2}} ((\Sigma_1 - \Sigma_2)^2 + (\Sigma_1 - \Sigma_3)^2 + (\Sigma_2 - \Sigma_3)^2)^{1/2} \tag{11}$$

132 Relations, Eq. (10) and Eq. (11) allows to express $\Sigma_1, \Sigma_2, \Sigma_3$ as functions of Σ_{eq}, T and L ,
133 with the range of possible values:

$$0 \leq \Sigma_e \leq \infty, \quad -\infty \leq T \leq \infty, \quad -1 \leq L \leq 1 \tag{12}$$

134 In this work, the stress states are characterized by the values of the stress triaxiality, T , and
135 the Lode parameter L , while the strain states are characterized by the equivalent strain in the
136 band, E_{eq}^b , and the macroscopic equivalent strain, E_{eq} , in the upper/lower faces of the outer blocks.
137 Finite element unit cell calculations are carried out for prescribed constant stress triaxiality, T , and
138 Lode parameter, L , values using the commercial finite element code ABAQUS/Standard (2017).
139 The periodic boundary conditions on the faces of the unit cell are implemented as multi-point

140 constraints in ABAQUS/Standard (2017), while the boundary conditions required to prescribe
 141 constant values of T and L are implemented in ABAQUS/Standard (2017) using an MPC user
 142 defined subroutine. More details of the boundary conditions to prescribe constant values of T and
 143 L are given in Appendix A. The finite element calculations use C3D20R elements from the in-built
 144 element library of ABAQUS/Standard (2017), and the number of elements in the finite element
 145 mesh varies from 9,672 to 18,316 for initial band angle varying from $\psi_u = 0^\circ$ to 39° , respectively.
 146 A cropped region of a unit cell with $\psi_u = 39^\circ$, $f_0 = 0.001$ and $D_0 = 1 \text{ mm}$ with finite element
 147 mesh in the voided region is shown in Fig. 1.

148 2.2. Constitutive Relation

149 The matrix material of the unit cell is modeled using finite strain J_2 flow theory. In the
 150 finite element calculations, updated Lagrangian formulation is used to account for large deforma-
 151 tions. For hypo elastic-plastic materials, the macroscopic rate of plastic deformation tensor, $\dot{\mathbf{E}}^p$,
 152 is assumed to be related to the macroscopic stress rate by:

$$\dot{\Sigma} = \mathbf{C} : (\dot{\mathbf{E}} - \dot{\mathbf{E}}^p) \quad (13)$$

153 where, \mathbf{C} is the linear isotropic elastic tensor defined by the fourth order tensorial relation:

$$\mathbf{C} = 2G\mathbf{I}_{dev} + K\mathbf{1} \otimes \mathbf{1} \quad (14)$$

154 with \mathbf{I}_{dev} being the unit deviatoric fourth order tensor having the form,

$$(\mathbf{I}_{dev})_{ijkl} = 1/2(\delta_{ik}\delta_{jl} + \delta_{il}\delta_{jk}) - 1/3\delta_{ij}\delta_{kl} \quad (15)$$

155 while $G = E/(2(1 + \nu))$ and $K = E/(3(1 - 2\nu))$ are elastic constants.

156 Assuming Mises plasticity, the yield function and the associated flow rule are given as:

$$\begin{aligned} \Psi &= \Sigma_{eq} - \bar{\sigma}(\dot{\varepsilon}^p) \\ \dot{\mathbf{E}}^p &= \dot{\lambda} \frac{\partial \Psi}{\partial \dot{\Sigma}} \end{aligned} \quad (16)$$

157 where, $\bar{\sigma}$ follows:

$$\bar{\sigma} = \begin{cases} E\varepsilon & \varepsilon \leq \varepsilon_0 \\ \sigma_0 \cdot (1 + (\frac{\dot{\varepsilon}^p}{\dot{\varepsilon}_0})^m) & \varepsilon > \varepsilon_0 \end{cases} \quad (17)$$

158 In Eq. (17), σ_0 represents a reference yield stress, m is the strain rate sensitivity parameter
 159 of the material, $\dot{\varepsilon}_0$ is the reference strain rate, E is the Young's modulus, $\varepsilon_0 = \sigma_0/E$, and plastic
 160 equivalent strain rate, $\dot{\varepsilon}^p = \sqrt{\frac{2}{3}\dot{\mathbf{E}}^p : \dot{\mathbf{E}}^p}$.

161 **3. Results and Discussion**

162 In a porous ductile material, onset of macroscopic localization due to the softening induced by
 163 void nucleation and growth, or due to void coalescence resulting from plastic strain localization
 164 in the ligaments between the voids, marks the end of uniform deformation. For a strain rate
 165 independent porous ductile material, Tekoğlu et al. (2015) showed that depending on the value
 166 of the imposed stress triaxiality a clear separation exists between the two modes of macroscopic
 167 localization. This raises a fundamental question: how does the material’s strain rate sensitivity
 168 affect the two modes of localization or ductile failure as a function of the imposed stress triaxiality?
 169 In this section, we present results obtained using the numerical method detailed under Section 2
 170 to address this question.

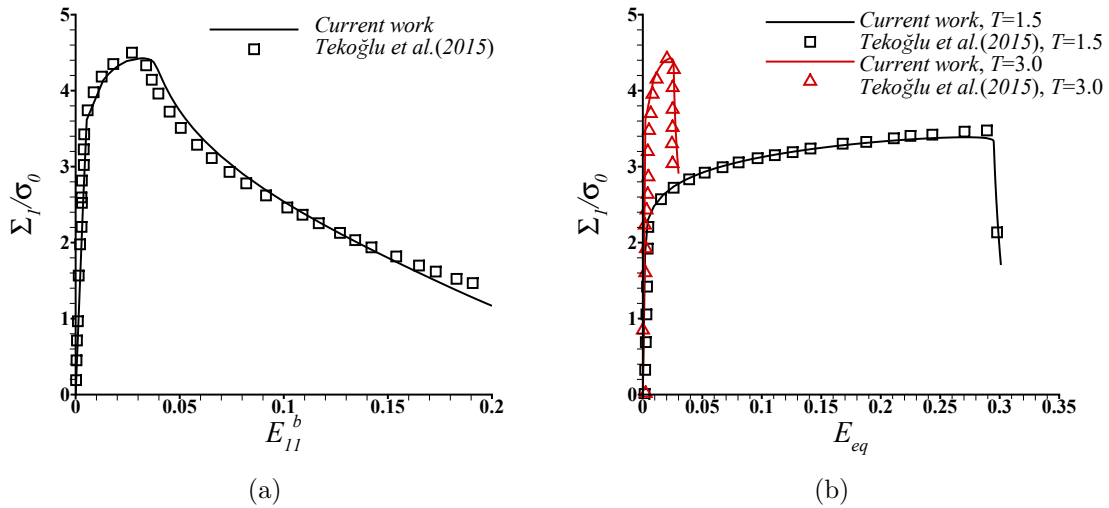


Figure 2: Comparison of the evolution of (a) normalized Σ_1/σ_0 with E_{11}^b for $T = 3.0$ and that of (b) Σ_1/σ_0 with E_{eq} for $T = 1.5$ and $T = 3.0$, predicted in the current work with the results of Tekoğlu et al. (2015). In both (a) and (b), $L = -1$, $\psi_u = 0^\circ$, $f_0 = 0.001$ and $N = 0.1$.

171 Our numerical method to model the unit cell that includes a central block with a single void
 172 in its center within two void-free semi-infinite blocks, differs from that of Tekoğlu et al. (2015).
 173 Tekoğlu et al. (2015) only considered the inclined part of the unit cell within the band, Fig. 1,
 174 and modeled the void-free semi-infinite block (along x_1) through complex boundary conditions.
 175 On the other hand, here we assume that (see Section 2) if the length of the void-free block along
 176 x_1 is sufficiently greater than the characteristic length, D_0 , of the unit cell, it can mimic the semi-
 177 infinite block. Thus, it is warranted to validate the predictions of our numerical method against
 178 the available results of Tekoğlu et al. (2015). To this end, we use a strain rate independent flow
 179 response, as in Tekoğlu et al. (2015):

$$\bar{\sigma} = \begin{cases} E\varepsilon & \varepsilon \leq \varepsilon_0 \\ \sigma_0 \cdot \left(\frac{\varepsilon^p}{\varepsilon_0^p}\right)^N & \varepsilon > \varepsilon_0 \end{cases} \quad (18)$$

180 instead of Eq. (17). The calculations use, $E = 167GPa$, $\sigma_0 = 418MPa$, $\varepsilon_0 = 0.0025$, $\nu = 0.3$
 181 and $N = 0.1$. The evolution of the normalized macroscopic stress along x_1 , Σ_1/σ_0 , with the strain

182 in the band, E_{11}^b , for $T = 3.0$, $L = -1$, $\psi_u = 0^\circ$ and $f_0 = 0.001$ predicted using the numerical
 183 method detailed under Section 2 are compared with the results of Tekoğlu et al. (2015) in Fig. 2(a).
 184 Similarly, the evolution of Σ_1/σ_0 with the macroscopic equivalent strain in the outer blocks, E_{eq} ,
 185 for $T = 1.5$ and 3.0 , and the same values of L , ψ_u and f_0 predicted using the current method
 186 are compared with the results of Tekoğlu et al. (2015) in Fig. 2(b). The results (of the current
 187 work) presented in Fig. 2, are for a unit cell whose length along x_1 direction is six times the
 188 characteristic length, D_0 , of the problem i.e. $L_{10} = 6D_0$. The strikingly good correlation between
 189 the predictions using our method and the results of Tekoğlu et al. (2015) in Fig. 2, clearly shows
 190 that the assumption of $L_{10} = 6D_0$ numerically represent the unit cell consisting of a central block
 191 with a single void in its center within two void-free semi-infinite blocks.

192 After validating our numerical method, we now focus on analyzing the influence of material's
 193 strain rate sensitivity on the onset of macroscopic localization due to void growth induced soft-
 194 ening and/or void coalescence. All the results presented here onwards are from the finite element
 195 calculations utilizing strain rate dependent flow response defined in Eq. (17). The full set of con-
 196 stitutive parameters used to define material (in the band as well as in the outer block) in the
 197 calculations are: $E = 167GPa$, $\nu = 0.3$, $\sigma_0 = 418MPa$, $\varepsilon_0 = 0.0025$, and $\dot{\varepsilon}_0 = 1 s^{-1}$, while
 198 the strain rate sensitivity parameter, m , is varied from 0 to 0.25. For each strain rate sensitivity
 199 parameter value, unit cells with one initial void volume fraction, $f_0 = 0.001$, but three initial
 200 orientations of the voided band, $\psi_u = 0^\circ$, 20° and 39° are considered. The choice of the initial
 201 orientation of the voided band, ψ_u , is based on the results of Tekoğlu et al. (2015) for strain
 202 rate independent material. Finally, for each strain rate sensitivity parameter, m , value and ini-
 203 tial orientation of the voided band, ψ_u , calculations are carried out for prescribed constant stress
 204 triaxiality, T , values in the range, $0.75 \leq T \leq 3$ and one Lode parameter, $L = -1$.

205 3.1. Strain Localization, Void Growth and Void Coalescence

206 The evolution of the equivalent strain inside the band, E_{eq}^b , with the macroscopic equivalent
 207 strain outside the band, E_{eq} , in unit cells with initial orientation of the voided band, $\psi_u = 0^\circ$ and
 208 39° are shown in Fig. 3. As shown in Figs. 3, during initial stages of deformation E_{eq}^b is same as
 209 E_{eq} , but at later stages of deformation, strain localizes in the band, and thereafter E_{eq}^b increases
 210 rapidly while E_{eq} increases slightly in the material outside the band. The onset of localization is
 211 assumed to occur when the ratio between the rate of macroscopic equivalent strain in the band
 212 and outside the band reach the value of 5. The onset of void coalescence is assumed to occur when
 213 the ratio of the maximum to the minimum equivalent plastic strain rate at the void surface first
 214 exceeds the threshold of 20, as in Tekoğlu et al. (2015). For $T = 1.25$, the onset of coalescence
 215 occurs soon after the onset of localization. But, for $T = 2.75$, the onset of coalescence occurs
 216 at a much greater value of E_{eq}^b following the onset of localization. A comparison of the results
 217 shown in Figs. 3(a) and (b), and Figs. 3(c) and (d), show that increasing the strain rate sensitivity
 218 of the material delays the onset of both, the localization and coalescence. However, the relative
 219 stabilizing effect of material's strain rate sensitivity is greater at the onset of localization than at
 220 the onset of void coalescence. For example, for $T = 2.75$, $(E_{eq}^b)_{m=0.25}/(E_{eq}^b)_{m=0} \approx 5.3$ at the onset
 221 of localization and $(E_{eq}^b)_{m=0.25}/(E_{eq}^b)_{m=0} \approx 2.8$ at the onset of void coalescence. Also a comparison
 222 of the results shown in Figs. 3(a) and (c), and Figs. 3(b) and (d), show that there is an increase in
 223 the relative stabilizing effect of material's strain rate sensitivity with the increasing value of the
 224 imposed stress triaxiality.

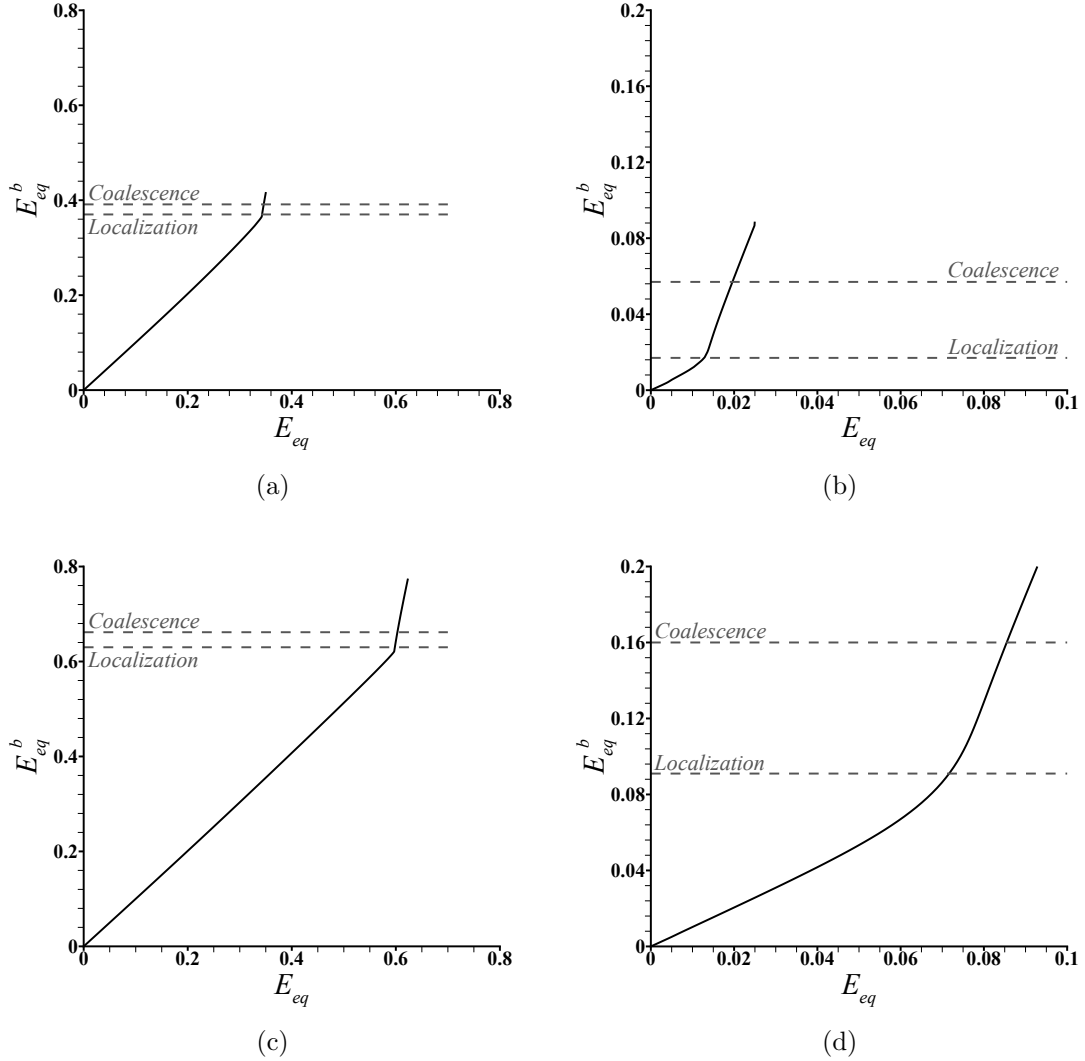


Figure 3: Evolution of equivalent strain in the band, E_{eq}^b , with macroscopic equivalent strain outside the band, E_{eq} , for (a) imposed stress triaxiality, $T = 1.25$ and strain rate sensitivity parameter, $m = 0$, (b) $T = 2.75$ and $m = 0$, (c) $T = 1.25$ and $m = 0.25$, and (d) $T = 2.75$ and $m = 0.25$. The initial orientation of the voided band is $\psi_u = 0^\circ$ for the cases shown in (a) and (c), and $\psi_u = 39^\circ$ for the cases shown in (b) and (d). In the figures the value of E_{eq}^b at the onset of localization and void coalescence are marked with dashed horizontal lines.

225 The evolution of normalized porosity, f/f_0 , with macroscopic equivalent strain outside the
 226 band, E_{eq} , for $T = 1.25$, is shown for two unit cells with initial orientation of the voided band
 227 $\psi_u = 0^\circ$ and $\psi_u = 39^\circ$ in Figs. 4(a) and (c), respectively. The same is shown for $T = 2.5$, for two
 228 unit cells with $\psi_u = 0^\circ$ and $\psi_u = 39^\circ$ in Figs. 4(b) and (d), respectively. To quantify the influence
 229 of the strain rate sensitivity parameter on the evolution of the porosity, results are shown in Fig. 4
 230 for $m = 0, 0.05$, and 0.1 . As shown in Fig. 4, for both the values of T and ψ_u , a higher value of
 231 m shifts the f/f_0 versus E_{eq} curves to the right i.e. the stabilizing effect of the material's strain
 232 rate sensitivity slows down the evolution of porosity. For $T = 2.5$, the value of f/f_0 at the onset
 233 of localization is less than the value of f/f_0 at the onset of void coalescence for both the values

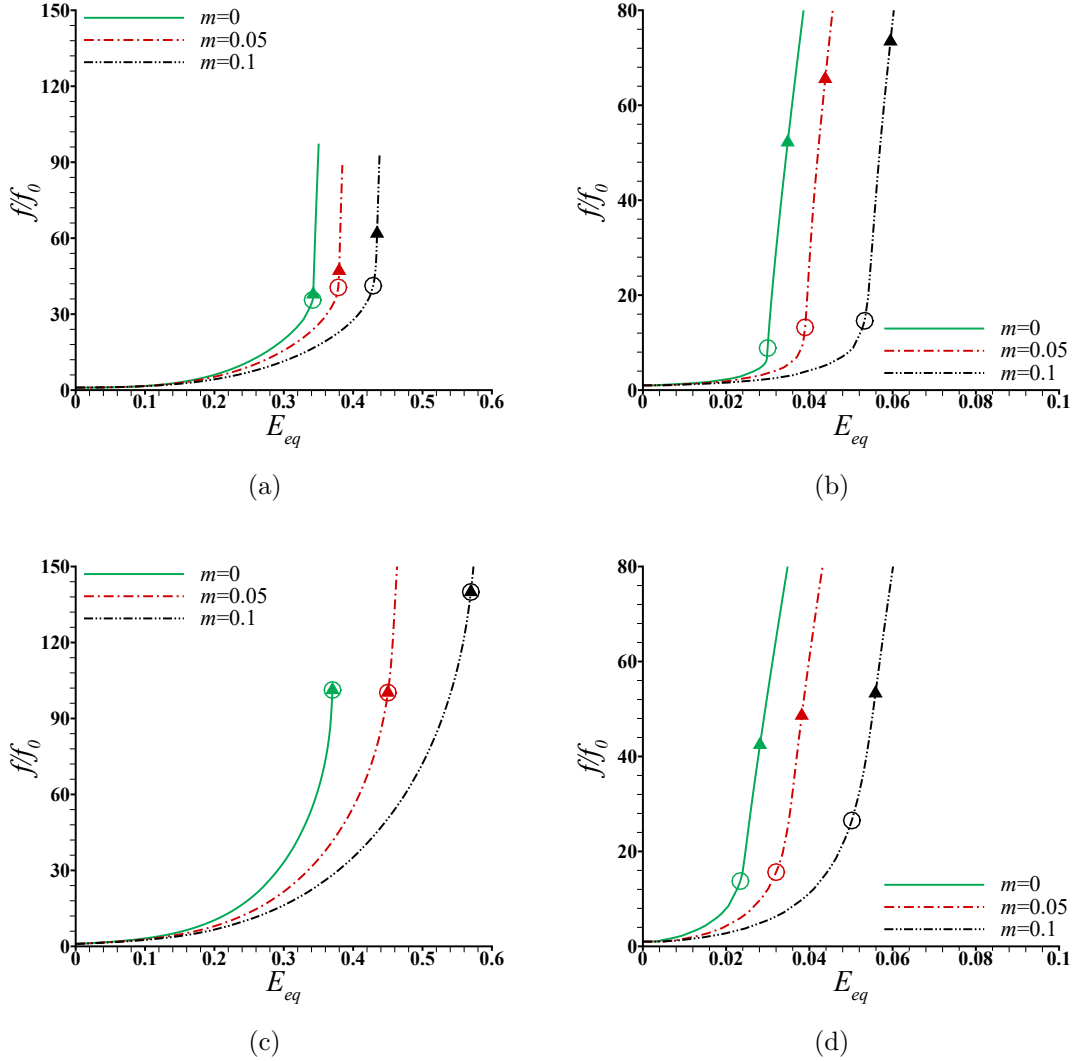


Figure 4: Evolution of the normalized porosity, f/f_0 , with E_{eq} for (a) $\psi_u = 0^\circ$ and $T = 1.25$, (b) $\psi_u = 0^\circ$ and $T = 2.5$, (c) $\psi_u = 39^\circ$ and $T = 1.25$, and (d) $\psi_u = 39^\circ$ and $T = 2.5$. The open circles in the figure mark the onset of localization while the closed triangles mark the onset of void coalescence.

234 of ψ_u and all three values of m . For $T = 1.25$, the value of f/f_0 at the onset of localization is
 235 less than the value of f/f_0 at the onset of void coalescence for $\psi_u = 0^\circ$ for $m > 0$. However, for
 236 $T = 1.25$, the value of f/f_0 at the onset of localization is same as the value of f/f_0 at the onset
 237 of void coalescence for $\psi_u = 39^\circ$ for all three values of m .

238 The effect of the material's strain rate sensitivity on deformation in the band and distribution
 239 of equivalent plastic strain on the void surface is highlighted in Fig. 5. In Fig. 5, results are
 240 shown for two strain rate sensitivity parameters, $m = 0$ and 0.25 , for a unit cell with the initial
 241 orientation of the band, $\psi_u = 20^\circ$ and subjected to an imposed stress triaxiality, $T = 1.0$. As
 242 can be seen in Fig. 5, the edges, ad and bc , that were initially straight and normal to the x_3 axis,
 243 undergo deformation following the periodicity of the initial voids in the band. In addition, the
 244 results also show that at the same equivalent strain levels in the band, E_{eq}^b , the maximum value

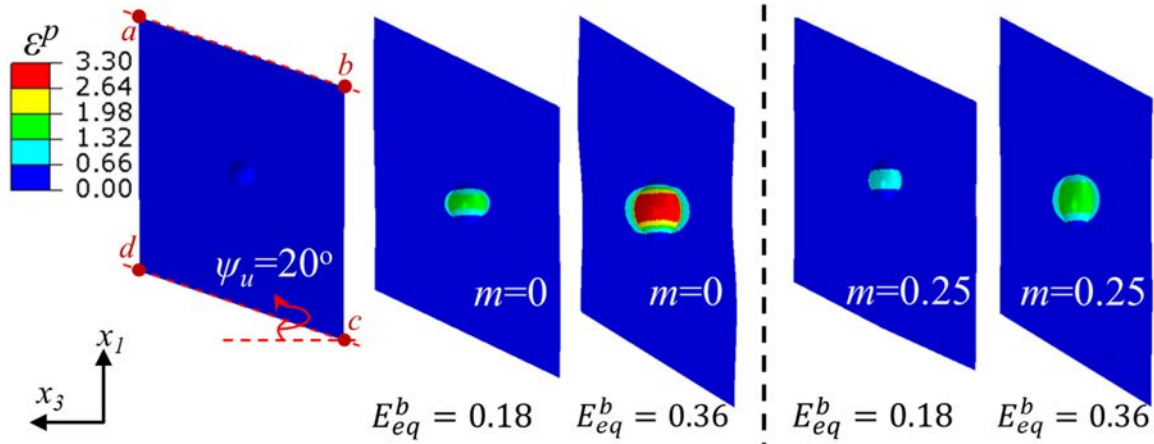


Figure 5: Deformed shape of the band and the distribution of the equivalent plastic strain, ε^p , in the band with initial orientation $\psi_u = 20^\circ$ under imposed stress triaxiality $T = 1.0$ for two strain rate sensitivity parameters, $m = 0$ and 0.25 at two equivalent strain levels in the band, $E_{eq}^b = 0.18$ and 0.36 .

245 of equivalent plastic strain, ε^p , on the void surface for $m = 0.25$ is much less than that for $m = 0$.
 246 The lower levels of ε^p on the void surface for $m = 0.25$ compared to $m = 0$ is consistent with the
 247 effect of m on the evolution of f/f_0 shown in Fig. 4.

248 *3.2. Effect of Strain Rate Sensitivity on Critical Porosity*

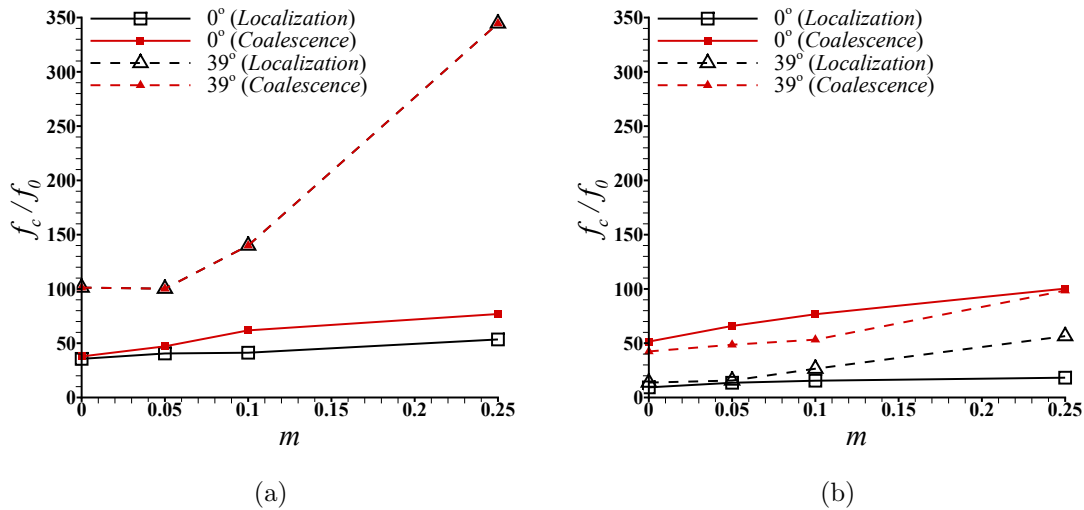


Figure 6: Variation of the normalized critical value of porosity, f_c/f_0 , at the onset of localization and void coalescence with material's strain rate sensitivity parameter, m , for (a) $T = 1.25$ and (b) $T = 2.5$.

249 We now analyze the effect of material's strain rate sensitivity, m , on critical values of porosity
 250 at the onset of strain localization and void coalescence. The critical value of porosity at the onset
 251 of void coalescence is widely used as an input parameter to simulate ductile fracture due to void
 252 nucleation, growth and coalescence (Besson et al., 2003; Srivastava et al., 2014; Cheng et al., 2014).

253 The variation of the normalized critical value of porosity, f_c/f_0 , at the onset of localization
254 and void coalescence with material's strain rate sensitivity parameter, m , in two unit cells with
255 initial orientation of the voided band, $\psi_u = 0^\circ$ and 39° , for two values of imposed stress triaxiality,
256 $T = 1.25$ and 2.5 , are shown in Fig. 6. For $T = 1.25$ and $\psi_u = 0^\circ$, the values of f_c/f_0 at the onset
257 of localization and void coalescence are roughly the same for $m < 0.05$. However, for greater value
258 of m the value of f_c/f_0 at the onset of localization is less than the value of f_c/f_0 at the onset
259 of void coalescence. For $T = 1.25$ and $\psi_u = 39^\circ$, the values of f_c/f_0 at the onset of localization
260 and void coalescence are roughly the same for all values of m . On the other hand, for $T = 2.5$,
261 the values of f_c/f_0 at the onset of localization is less than the values of f_c/f_0 at the onset of void
262 coalescence for all values of m , for both $\psi_u = 0^\circ$ and 39° . Also, for $T = 2.5$ the difference between
263 the values of f_c/f_0 at the onset of localization and void coalescence increases with increasing value
264 of m . The results presented in Fig. 6 show that at low imposed stress triaxiality values, the
265 extent of void growth induced softening is not sufficient to trigger macroscopic localization, thus
266 localization does not occur until the onset of void coalescence. On the other hand, the void growth
267 induced softening is sufficient to trigger macroscopic localization at high imposed stress triaxiality
268 values and the macroscopic localization occurs much before the void coalescence. The increase
269 in the value of f_c with increasing value of m is because an increase in the value of m results in
270 increased strain rate hardening thus requiring an increase in damage induced softening to trigger
271 any localized deformation in the voided band or within the ligament between the neighboring
272 voids to trigger void coalescence.

273 3.3. Effect of Strain Rate Sensitivity on Critical Strain

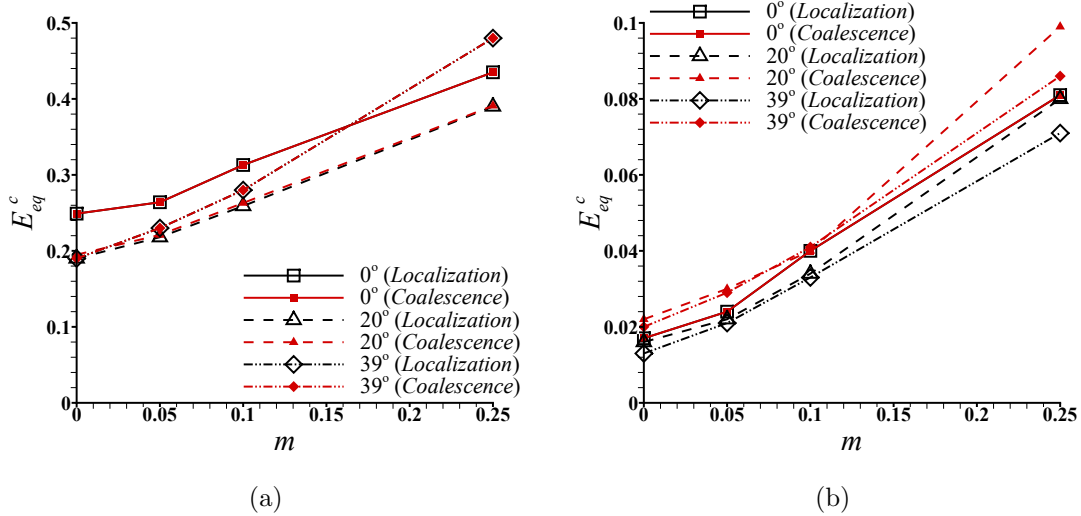


Figure 7: Variation of the critical macroscopic equivalent strain, E_{eq}^c , outside the band at the onset of localization/coalescence with material's strain rate sensitivity parameter, m , for (a) $T = 1.5$ and (b) $T = 2.75$.

274 The results presented thus far clearly show that both the material's strain rate sensitivity and
275 imposed stress triaxiality affect the onset of strain localization and void coalescence. Following
276 this, we analyze the variation of critical macroscopic equivalent strain outside the band, E_{eq}^c , and
277 critical equivalent strain inside the band, E_{eq}^{cb} , with strain rate sensitivity parameter, m , shown in

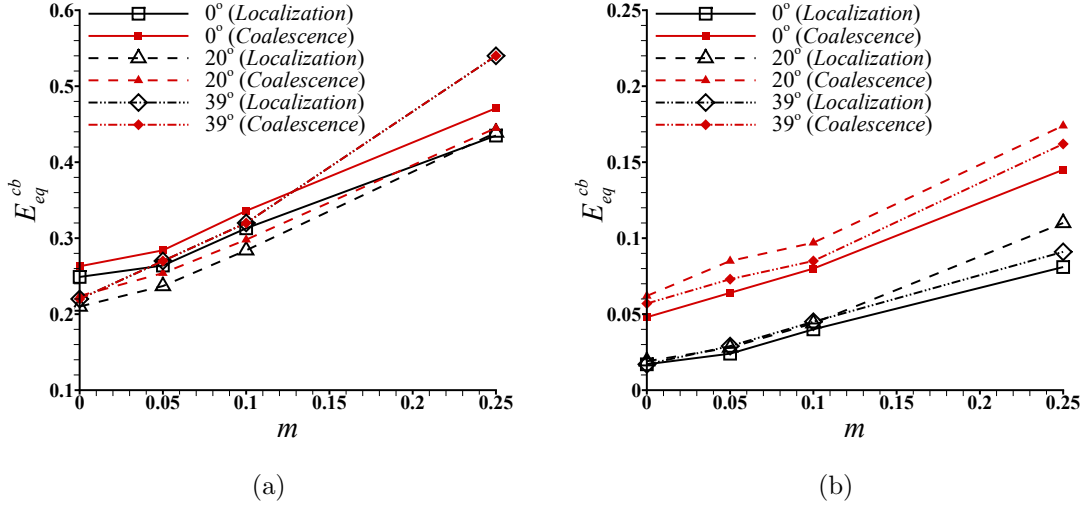


Figure 8: Variation of the critical equivalent strain, E_{eq}^{cb} , inside the band at the onset of localization/coalescence with material's strain rate sensitivity parameter, m , for (a) $T = 1.5$ and (b) $T = 2.75$.

278 Figs. 7 and 8, respectively, and the variation of E_{eq}^{cb} with imposed stress triaxiality, T , shown in
 279 Fig. 9.

280 As shown in Fig. 7, the value of E_{eq}^c increases with increasing value of strain rate sensitivity
 281 parameter, m , for all three initial orientation of the voided band, $\psi_u = 0^\circ$, 20° and 39° , and
 282 for both the imposed stress triaxiality values, $T = 1.5$ and 2.75 . As also shown in the figure,
 283 for all three ψ_u values and for $T = 1.5$, the value of E_{eq}^c is same at the onset of localization
 284 and void coalescence. For $T = 2.75$, E_{eq}^c values at void coalescence are slightly greater than the
 285 values of E_{eq}^c at the onset of localization. This is consistent with the observation that at low
 286 imposed stress triaxiality values, the extent of void growth induced softening is not sufficient to
 287 trigger macroscopic localization, whereas at high imposed stress triaxiality values the void growth
 288 induced softening is sufficient to trigger macroscopic localization. As also shown in Fig. 7, the
 289 effect of initial band orientation on the value of E_{eq}^c depends on both, the values of T and m .
 290 For example, the minimum value of E_{eq}^c at the onset of localization corresponds to $\psi_u = 20^\circ$ for
 291 $T = 1.5$ while it corresponds to $\psi_u = 39^\circ$ for $T = 2.75$.

292 Similarly, the value of the critical equivalent strain in the band, E_{eq}^{cb} , at the onset of localiza-
 293 tion/coalescence increases with increasing value of m for all three ψ_u and for both T , Fig. 8. In
 294 addition, the variation of E_{eq}^{cb} with m for $T = 1.5$, Fig. 8(a), roughly follows the same trend as
 295 shown in Fig. 7(a) for E_{eq}^c . But for $T = 2.75$, the value of E_{eq}^{cb} at the onset of localization is less
 296 than the value of E_{eq}^{cb} at the onset of void coalescence for all the values of m and ψ_u , Fig. 8(b).
 297 For $T = 2.75$, the initial band orientation that gives lowest values of E_{eq}^{cb} is $\psi_u = 0^\circ$, and the
 298 orientation that gives largest values of E_{eq}^{cb} is $\psi_u = 20^\circ$. This is in contrast to the dependence of
 299 E_{eq}^c on ψ_u as shown in Fig. 7(b). This is because at high imposed stress triaxiality values, the
 300 onset of macroscopic localization occurs due to void growth induced softening that significantly
 301 affects the deformation in the band.

302 Figures 9(a) and (b) compare the variation of E_{eq}^{cb} at the onset of localization and coalescence,
 303 with imposed stress triaxiality values, T , for $m = 0.05$ and 0.25 , respectively. As shown in

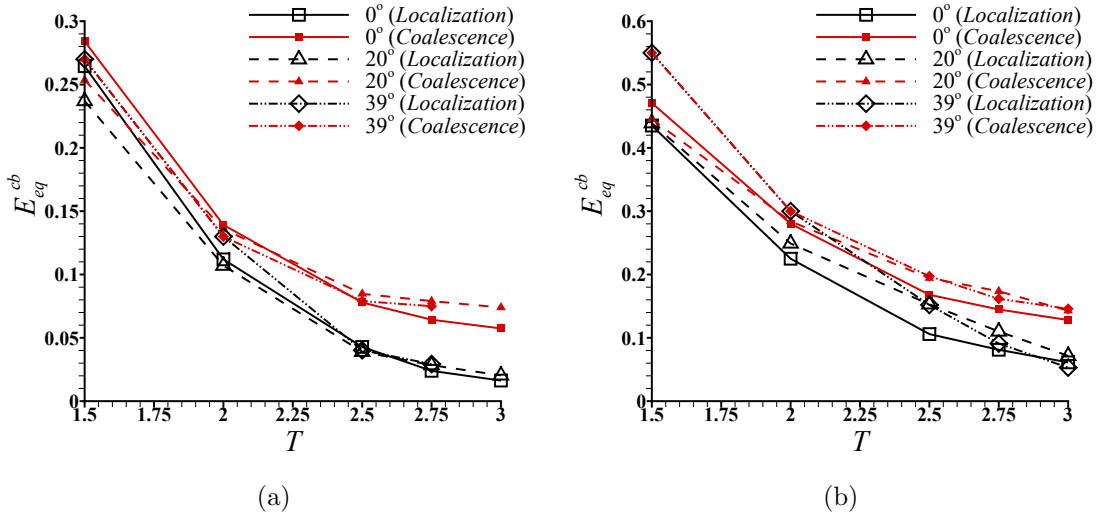


Figure 9: Variation of the critical equivalent strain, E_{eq}^{cb} , inside the band at the onset of localization/coalescence with imposed stress triaxiality, T , for (a) $m = 0.05$ and (b) $m = 0.25$.

4

304 the figure, for both the values of m , the value of E_{eq}^{cb} at localization/coalescence decreases with
 305 increasing value of the imposed T . But for sufficiently large values of T , with increasing T ,
 306 the decrease in E_{eq}^{cb} at void coalescence is rather gradual as compared to the decrease in E_{eq}^{cb}
 307 at localization. This results in a clear separation between the values of E_{eq}^{cb} at localization and
 308 coalescence for $T \geq 2$, with the increasing difference between E_{eq}^{cb} at localization and coalescence
 309 with increasing value of T .

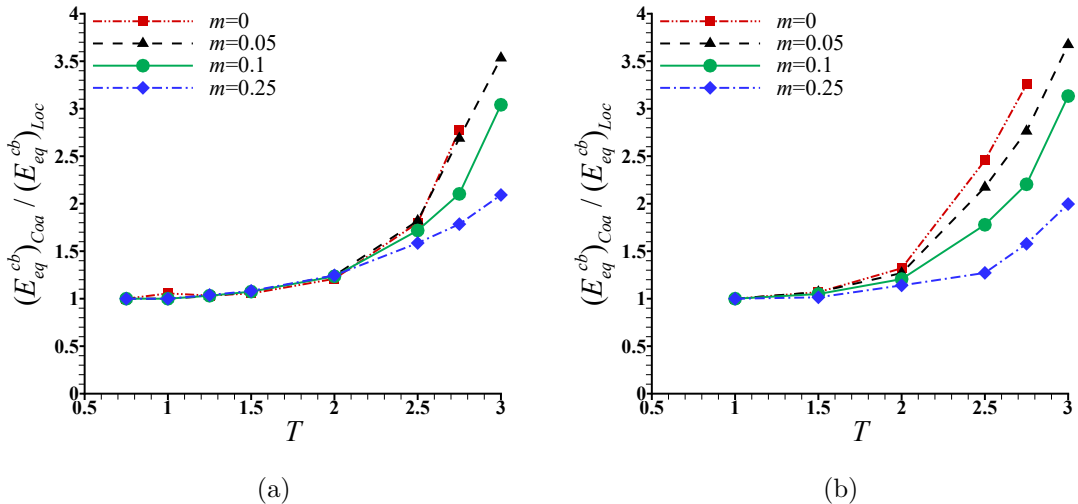


Figure 10: Variation in the ratio $(E_{eq}^{cb})_{Coa} / (E_{eq}^{cb})_{Loc}$ with imposed stress triaxiality values, T , for initial orientation of the voided band, (a) $\psi_u = 0^\circ$ and (b) $\psi_u = 20^\circ$.

310 We now analyze the variation of the critical equivalent strain in the band at the onset of

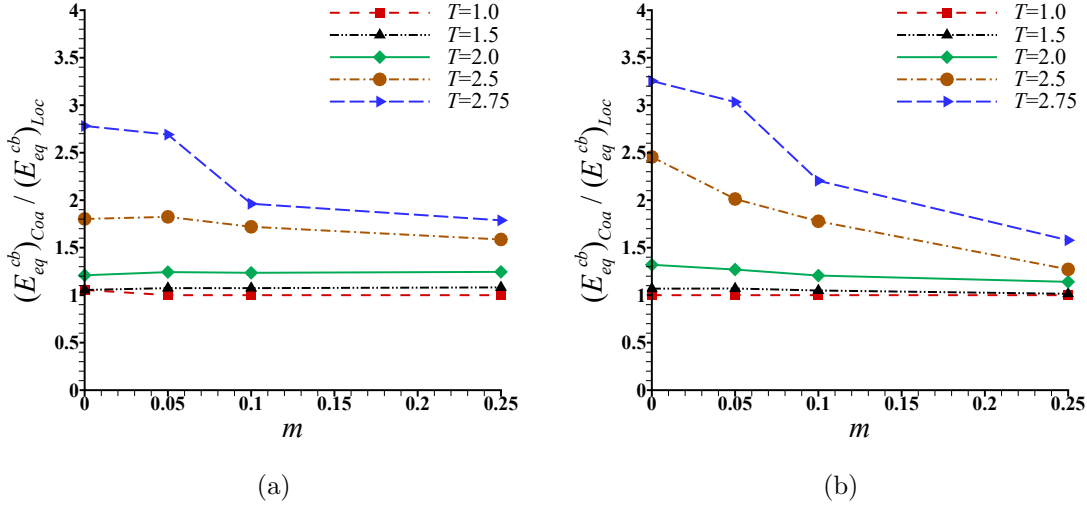


Figure 11: Variation in the ratio $(E_{eq}^{cb})_{Cooa} / (E_{eq}^{cb})_{Loc}$ with material's strain rate sensitivity parameter, m , for initial orientation of the voided band, (a) $\psi_u = 0^\circ$ and (b) $\psi_u = 20^\circ$.

311 coalescence normalized with the value of the critical equivalent strain in the band at the onset
312 of localization, $(E_{eq}^{cb})_{Cooa} / (E_{eq}^{cb})_{Loc}$, with T and m in Figs. 10 and 11, respectively, for two initial
313 orientation of the voided band, ψ_u . As shown in Fig. 10, for all m and for both the values
314 of ψ_u , the ratio $(E_{eq}^{cb})_{Cooa} / (E_{eq}^{cb})_{Loc}$ is approximately one for $T < 2$ and for $T \geq 2$, the ratio
315 $(E_{eq}^{cb})_{Cooa} / (E_{eq}^{cb})_{Loc}$ increases with increasing value of T . This is because both $(E_{eq}^{cb})_{Cooa}$ and $(E_{eq}^{cb})_{Loc}$
316 decrease with increasing T but for $T \geq 2$, $(E_{eq}^{cb})_{Loc}$ decreases more rapidly with increasing T than
317 $(E_{eq}^{cb})_{Cooa}$. Furthermore, as shown in Fig. 11, for $T > 2$, the value of $(E_{eq}^{cb})_{Cooa} / (E_{eq}^{cb})_{Loc}$ decreases
318 with increasing m for both the values of ψ_u . The decrease in the value of $(E_{eq}^{cb})_{Cooa} / (E_{eq}^{cb})_{Loc}$ with
319 increasing m becomes more pronounced with increasing value of the imposed T . Note, that both
320 $(E_{eq}^{cb})_{Cooa}$ and $(E_{eq}^{cb})_{Loc}$ increase with increasing m , thus a decrease in the value of $(E_{eq}^{cb})_{Cooa} / (E_{eq}^{cb})_{Loc}$
321 suggests that $(E_{eq}^{cb})_{Loc}$ increases more rapidly with increasing m for higher stress triaxiality values.
322 To summarize, the relative stabilizing effect induced by strain rate sensitivity of the material not
323 only increases with the increasing value of the imposed stress triaxiality, but also the relative
324 stabilizing effect of the strain rate sensitivity is greater at the onset of strain localization than at
325 the onset of void coalescence.

326 3.4. Effect of Strain Hardening

327 In this work, we have focused on answering the question: How does the materials strain rate
328 sensitivity affect the two mechanisms of macroscopic localization or ductile failure as a function
329 of the imposed stress triaxiality? To answer this question, we have carried out a series of unit
330 cell calculations, where the matrix material of the unit cell is considered to follow a strain rate
331 dependent elastic perfectly plastic flow response. So the question arises as to what extent strain
332 hardening in the material affects our results. A complete study of the combined effect of material's
333 strain rate sensitivity, strain hardening and imposed stress triaxiality is beyond the scope of this
334 work. However, our limited unit cell calculations presented in this section show that incorporating
335 both material's strain rate sensitivity and strain hardening does not affect the qualitative effect

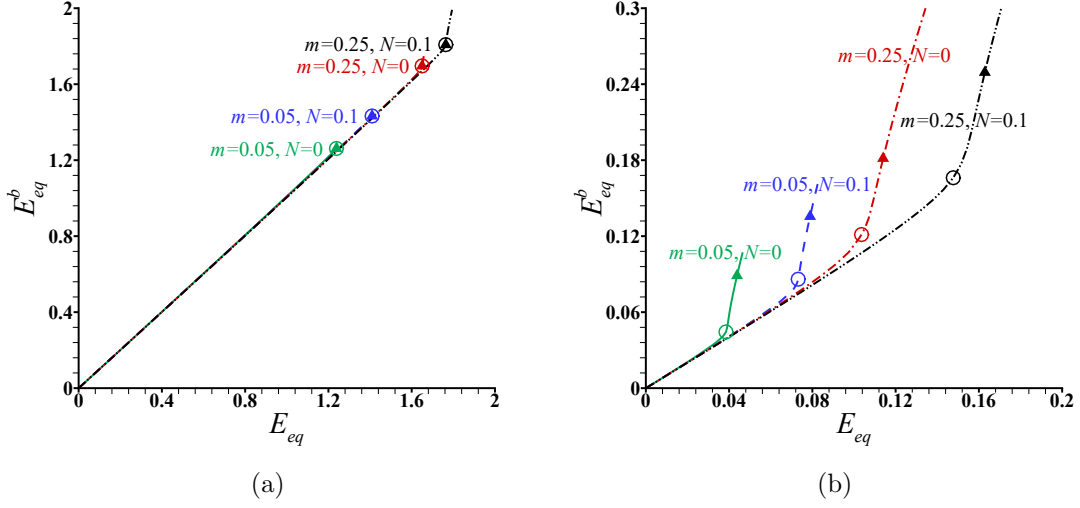


Figure 12: A comparison of the evolution of equivalent strain in the band, E_{eq}^b , with macroscopic equivalent strain outside the band, E_{eq} , in strain hardening and non strain hardening materials for (a) imposed stress triaxiality, $T = 0.75$ and (b) $T = 2.5$. The initial orientation of the voided band is $\psi_u = 0^\circ$ for all the cases shown. In the figures the open circles mark the onset of localization while the closed triangles mark the onset of void coalescence.

336 of material's strain rate sensitivity and stress triaxiality reported in this work.

337 The results of our limited unit cell calculations to explore the combined effect of material's
 338 strain rate sensitivity, strain hardening and stress triaxiality on the two mechanisms of macroscopic
 339 localization is shown in Fig. 12. The combined effect of material's strain rate sensitivity and strain
 340 hardening is explored using the flow response given as,

$$\bar{\sigma} = \begin{cases} E\varepsilon & \varepsilon \leq \varepsilon_0 \\ \sigma_0 \cdot \left(\frac{\varepsilon^p}{\varepsilon_0^p}\right)^N \cdot \left(1 + \left(\frac{\dot{\varepsilon}^p}{\dot{\varepsilon}_0^p}\right)^m\right) & \varepsilon > \varepsilon_0 \end{cases} \quad (19)$$

341 instead of Eq. (17). For the calculations corresponding to results in Fig. 12, the values of
 342 $E = 167GPa$, $\sigma_0 = 418MPa$, $\varepsilon_0 = 0.0025$, $\dot{\varepsilon}_0 = 1 s^{-1}$, $N = 0$ and 0.1 , and $m = 0.05$ and 0.25
 343 are used in Eq. (19). The results presented in Fig. 12 show that incorporating strain hardening
 344 in to the flow response of the material does not affect the qualitative effect of material's strain
 345 rate sensitivity and stress triaxiality on the onset of localization and void coalescence reported in
 346 this work. For example, irrespective of the value of the strain hardening exponent, N : (i) for low
 347 stress triaxiality value, $T = 0.75$, the value of E_{eq}^b at the onset of localization and void coalescence
 348 are the same, (ii) the value of E_{eq}^b at the onset of localization and void coalescence increases with
 349 the increasing value of strain rate sensitivity parameter, m , for both the values of T , (iii) for high
 350 stress triaxiality value, $T = 2.5$, the value of E_{eq}^b at the onset of localization is less than the value
 351 of E_{eq}^b at the onset of void coalescence, and (iv) the difference between the values of E_{eq}^b at the
 352 onset of localization and void coalescence decreases with increasing value of m .

353 4. Summary and Concluding Remarks

354 Strain localization and void coalescence (resulting in the formation of micro-cracks) in a porous
355 ductile material mark the end of uniform deformation and limits the ductility of the material. In
356 this work the focus is confined to analyzing the influence of material's strain rate sensitivity on
357 the onset of strain localization and void coalescence as a function of the imposed stress triaxiality.
358 To this end, three dimensional finite element calculations of unit cells have been carried out
359 to model localization and coalescence in an infinite block containing a periodic distribution of
360 initially spherical voids in a band. The unit cell modeled consists of a central block with a single
361 void in its center within two semi-infinite void-free blocks. The matrix material of the unit cell
362 is considered to follow a strain rate dependent elastic perfectly plastic flow response. **Limited**
363 **calculations have also been carried out to explore the combined effect of material's strain rate**
364 **sensitivity and strain hardening.** The unit cell calculations are carried out for one initial void
365 volume fraction ($f_0 = 0.001$), a range of strain rate sensitivity parameter (varying in the range
366 $0 \leq m \leq 0.25$), a range of imposed stress triaxiality (varying in the range $0.75 \leq T \leq 3$) with one
367 Lode parameter ($L = -1$), and three initial orientations of the voided band ($\psi_u = 0^\circ, 20^\circ$ and
368 39°). In the calculations, onset of localization is defined as the point in the deformation history
369 when the ratio of the rate of deformation in the band and outside the band reaches a critical level,
370 while the onset of coalescence is defined when the ratio of the maximum to the minimum effective
371 plastic strain rate at the surface of the void reaches a critical value following the work of Tekoğlu
372 et al. (2015). Our results show that both the critical void volume fraction and strain, at the onset
373 of localization and coalescence, are strongly influenced by the material's strain rate sensitivity and
374 the imposed stress triaxiality.

375 The main conclusions of this work are as follows:

- 376 1. Influence of material's strain rate sensitivity, m , and imposed stress triaxiality, T , on the
377 critical void volume fraction, f_c , at the onset of strain localization and void coalescence:
 - 378 (a) For low T values, f_c is roughly the same at the onset of localization and coalescence,
379 whereas for greater values of T , f_c at the onset of coalescence is greater than f_c at the
380 onset of localization.
 - 381 (b) For all values of T , the value of f_c at localization/coalescence increases with increasing
382 m .
- 383 2. Influence of material's strain rate sensitivity, m , and imposed stress triaxiality, T , on the
384 critical equivalent strain in the band, E_{eq}^{cb} , at the onset of strain localization and void coa-
385 luescence:
 - 386 (a) For low T values, $T < 2$, E_{eq}^{cb} is same at the onset of localization and coalescence,
387 whereas for $T \geq 2$, E_{eq}^{cb} at the onset of coalescence is greater than E_{eq}^{cb} at the onset of
388 localization.
 - 389 (b) For all values of m , the value of E_{eq}^{cb} at the onset of localization/coalescence decreases
390 with increasing T . But for $T \geq 2$, the value of E_{eq}^{cb} at localization decreases more
391 rapidly with increasing T compared to the value of E_{eq}^{cb} at coalescence.
 - 392 (c) For all values of T , the value of E_{eq}^{cb} at the onset of localization/coalescence increases
393 with increasing value of m . But for $T \geq 2$, the value of E_{eq}^{cb} at localization increases
394 more with increasing value of m compared to the value of E_{eq}^{cb} at coalescence.

395 (d) The concluding points, 2(b) and (c), clearly show that the relative stabilizing effect of
396 m increases with the increasing value of T , and the relative stabilizing effect of m is
397 greater at the onset of localization than at the onset of coalescence.

398 Our limited results aimed at exploring the combined effect of material's strain rate sensitivity,
399 strain hardening and imposed stress triaxiality on the onset of localization and void coalescence
400 show that incorporating strain hardening into the flow response of the material does not affect the
401 aforementioned qualitative effect of material's strain rate sensitivity and stress triaxiality on the
402 onset of localization and void coalescence. In this work, we have focused on one Lode parameter
403 value, $L = -1$. The value of the Lode parameter may also affect the onset of localization and
404 void coalescence especially at low values of stress triaxiality. The numerical method presented in
405 this work can be used for future research to explore the combined effect of material's strain rate
406 sensitivity and strain hardening, and imposed stress triaxiality and Lode parameter on the onset
407 of localization and void coalescence. Furthermore, our results motivate the need to incorporate
408 the effect of material's strain rate sensitivity in the porosity and stress triaxiality dependent flow
409 potential (or constitutive response) of the material.

410 Acknowledgements

411 The financial support provided by the European Union's Horizon2020 Programme (Excellent
412 Science, Marie-Sklodowska - Curie Actions, H2020 - MSCA - RISE - 2017) under REA grant
413 agreement 777896 (Project QUANTIFY) are gratefully acknowledged. Shmuel Osovski would also
414 like to acknowledge the financial support of the Pazy foundation (Young researchers award grant
415 no. 1176). We are thankful to Dr. J.A. Rodríguez-Martínez of University Carlos III of Madrid for
416 numerous fruitful discussions. The authors also acknowledge to Katarzyna Kowalczyk-Gajewska
417 from Institute of Fundamental Technological Research, Polish Academy of Sciences, for helpful
418 discussions.

419 **Appendix A. Procedure for the Multipoint constraint**

420 The procedure to prescribe proportional loading i.e. fixed ratio of principal stresses, $R = \Sigma_2/\Sigma_1$
 421 and $Q = \Sigma_3/\Sigma_1$ to maintain constant macroscopic stress triaxiality, T , and Lode parameter, L ,
 422 throughout the deformation history, follows the work of Vadillo et al. (2016).

423 Since the macroscopic true stresses $(\Sigma_1, \Sigma_2, \Sigma_3)$ and the macroscopic strain rates $(\dot{E}_1, \dot{E}_2, \dot{E}_3)$
 424 are equal to the volume average values in a cell (Hill, 1967), the total rate of deformation work in
 425 the whole cell \dot{W} considering jointly upper, lower and central voided block, can be written as:

$$\dot{W} = V\Sigma_1\dot{E}_1 + V\Sigma_2\dot{E}_2 + V\Sigma_3\dot{E}_3 \quad (\text{A.1})$$

426 where V is the total volume of the RVE.

427 Defining $P_1 = V\Sigma_1$, $P_2 = V\Sigma_2$ and $P_3 = V\Sigma_3$ as generalized forces and work rate conjugate
 428 quantities to \dot{E}_1 , \dot{E}_2 and \dot{E}_3 , respectively, the expression of \dot{W} becomes:

$$\dot{W} = P_1\dot{E}_1 + P_2\dot{E}_2 + P_3\dot{E}_3 \quad (\text{A.2})$$

429 in which P_1 , P_2 and P_3 must satisfy:

$$\frac{P_2}{P_1} = R; \quad \frac{P_3}{P_1} = Q \quad (\text{A.3})$$

430 The ratios R and Q can be written in terms of the imposed stress triaxiality, T , and Lode param-
 431 eter, L :

$$Q = \frac{3T\sqrt{L^2 + 3} - 3 - L}{3T\sqrt{L^2 + 3} + 3 - L}; \quad R = \frac{3T\sqrt{L^2 + 3} + 2L}{3T\sqrt{L^2 + 3} + 3 - L} \quad (\text{A.4})$$

432 Next, with the transformation:

$$\begin{pmatrix} \dot{E}_{(I)} \\ \dot{E}_{(II)} \\ \dot{E}_{(III)} \end{pmatrix} = \mathbf{N} \begin{pmatrix} \dot{E}_1 \\ \dot{E}_2 \\ \dot{E}_3 \end{pmatrix}; \quad \begin{pmatrix} P_{(I)} \\ P_{(II)} \\ P_{(III)} \end{pmatrix} = \mathbf{N} \begin{pmatrix} P_1 \\ P_2 \\ P_3 \end{pmatrix} \quad (\text{A.5})$$

433 where \mathbf{N} is an orthonormal ($\mathbf{N}^{-1} = \mathbf{N}^T$) unsymmetric matrix:

$$\mathbf{N} = \begin{pmatrix} A_{11} & A_{12} & A_{13} \\ A_{21} & A_{22} & A_{23} \\ A_{31} & A_{32} & A_{33} \end{pmatrix};$$

435 with the elements:

$$\begin{aligned} A_{11} &= \frac{1}{\sqrt{1 + R^2 + Q^2}}; & A_{12} &= \frac{R}{\sqrt{1 + R^2 + Q^2}}; & A_{13} &= \frac{Q}{\sqrt{1 + R^2 + Q^2}} \\ A_{21} &= -\frac{R}{\sqrt{1 + R^2}}; & A_{22} &= \frac{1}{\sqrt{1 + R^2}}; & A_{23} &= 0. \\ A_{31} &= \frac{Q}{\sqrt{(1 + R^2)(1 + R^2 + Q^2)}}; & A_{32} &= \frac{RQ}{\sqrt{(1 + R^2)(1 + R^2 + Q^2)}} \\ A_{33} &= -\frac{(1 + R^2)}{\sqrt{(1 + R^2)(1 + R^2 + Q^2)}} \end{aligned} \quad (\text{A.6})$$

436 Now, \dot{W} can be expressed in terms of the transformed rates of deformation and forces, as:

$$\dot{W} = P_{(I)}\dot{E}_{(I)} + P_{(II)}\dot{E}_{(II)} + P_{(III)}\dot{E}_{(III)} \quad (\text{A.7})$$

437 If in the transformed coordinate system, the imposed incremental boundary conditions are
438 prescribed as stress uniaxial:

$$P_{(II)} = 0; \quad P_{(III)} = 0; \quad \dot{E}_{(I)} = \dot{E}_I \quad (\text{A.8})$$

439 the total rate of deformation work has the form $\dot{W} = P_{(I)}\dot{E}_I$, that follows, in the initial system
440 and considering the relations given in Eq. (A.5), the three relations:

$$\begin{aligned} (1) \quad & P_{(II)} = 0 \rightarrow A_{21}P_1 + A_{22}P_2 + A_{23}P_3 = 0 \\ (2) \quad & P_{(III)} = 0 \rightarrow A_{31}P_1 + A_{32}P_2 + A_{33}P_3 = 0 \\ (3) \quad & \dot{E}_{(I)} = \dot{E}_I \rightarrow A_{11}\dot{E}_1 + A_{12}\dot{E}_2 + A_{13}\dot{E}_3 = \dot{E}_I \end{aligned} \quad (\text{A.9})$$

441 or in a similar manner, if values of R , Q and \dot{E}_I are prescribed on the unit cell, this leads to:

$$\begin{aligned} (1) \quad & (\Sigma_2/\Sigma_1) = R \\ (2) \quad & (\Sigma_3/\Sigma_1) = Q \\ (3) \quad & \left(\dot{E}_1 + R\dot{E}_2 + Q\dot{E}_3 \right) = \dot{E}_I \sqrt{1 + R^2 + Q^2} \end{aligned} \quad (\text{A.10})$$

442 This procedure was implemented into ABAQUS/Standard (2017) as MPC user subroutine.

443 **References**

- 444 ABAQUS/Standard, 2017. Simulia, User's Manual, version 6.17 Edition. Dassault Systèmes, Prov-
445 idence, USA.
- 446 Agoras, M., Ponte Castañeda, P., 2014. Anisotropic finite-strain models for porous viscoplastic
447 materials with microstructure evolution. *International Journal of Solids and Structures* 51, 981–
448 1002.
- 449 Aretz, H., 2007. Numerical analysis of diffuse and localized necking in orthotropic sheet metals.
450 *International Journal of Plasticity* 23, 798–840.
- 451 Barsoum, I., Faleskog, J., 2011. Micromechanical analysis on the influence of the lode parameter
452 on void growth and coalescence. *International Journal of Solids and Structures* 48 (6), 925–938.
- 453 Besson, J., Steglich, D., Brocks, W., 2003. Modeling of plane strain ductile rupture. *International*
454 *Journal of Plasticity* 19 (10), 1517–1541.
- 455 Brüning, M., Gerke, S., Hagenbrock, V., 2013. Micro-mechanical studies on the effect of the stress
456 triaxiality and the lode parameter on ductile damage. *International Journal of Plasticity* 50,
457 49–65.
- 458 Budiansky, B., Hutchinson, J., Slutsky, S., 1982. Void growth and collapse in viscous solids. in:
459 H.G. Hopkins and M.J. Sewell, eds., *Mechanics of Solids*, Pergamon Press, Oxford, 13–45.
- 460 Cheng, F., Kim, S.-M., Reddy, J., Al-Rub, R. K. A., 2014. Modeling of elastoplastic behavior of
461 stainless-steel/bronze interpenetrating phase composites with damage evolution. *International*
462 *Journal of Plasticity* 61, 94–111.
- 463 Cocks, A., Ashby, M., 1982a. Creep fracture by coupled power-law creep and diffusion under
464 multiaxial stress. *Metal Science* 16, 465–474.
- 465 Cocks, A., Ashby, M., 1982b. On creep fracture by void growth. *Progress in Material Science* 27,
466 189–244.
- 467 Czarnota, C., Mercier, S., Molinari, A., 2006. Modelling of nucleation and void growth in dynamic
468 pressure loading, application to spall test on tantalum. *International Journal of Fracture* 141,
469 177–194.
- 470 Dunand, M., Mohr, D., 2014. Effect of lode parameter on plastic flow localization after proportional
471 loading at low stress triaxialities. *Journal of the Mechanics and Physics of Solids* 66, 133–153.
- 472 Duva, J., 1986. A constitutive description of nonlinear materials containing voids. *Mechanics of*
473 *Materials* 5, 317–329.
- 474 Fressengeas, C., Molinari, A., 1985. Inertia and thermal effects on the localization of plastic flow.
475 *Acta Metallurgica* 33, 387–396.

- 476 Fritzen, F., Forest, S., Böhlke, T., Kondo, D., Kanit, T., 2012. Computational homogenization of
477 elasto-plastic porous metals. *International Journal of Plasticity* 29, 102–119.
- 478 Ghosh, A., 1977. Tensile instability and necking in materials with strain hardening and strain-rate
479 hardening. *Acta Metallurgica* 25, 1413–1424.
- 480 Guo, T., Wong, W., 2018. Void-sheet analysis on macroscopic strain localization and void coales-
481 cence. *Journal of the Mechanics and Physics of Solids* 118, 172–203.
- 482 Hill, R., 1967. The essential structure of constitutive laws for metal composites and polycrystals.
483 *Journal of the Mechanics and Physics of Solids* 15, 79–95.
- 484 Hutchinson, J., Neale, K., 1977. Influence of strain-rate sensitivity on necking under uniaxial
485 tension. *Acta Metall* 25, 839–846.
- 486 Hutchinson, J., Neale, K., Needleman, A., 1978. Sheet necking-I. validity of plane stress assump-
487 tions of the long wavelength approximation. In: Koistinen, D.P., Wang, N.W. (Eds.), *Mechanics*
488 *of Sheet Metal Forming*, New York: Plenum Publishing Corp, 111–126.
- 489 Koplík, J., Needleman, A., 1988. Void growth and coalescence in porous plastic solids. *Internation-
490 al Journal of Solids and Structures* 24 (8), 835–853.
- 491 Liu, Z., Wong, W., Guo, T., 2016. Void behaviors from low to high triaxialities: Transition from
492 void collapse to void coalescence. *International Journal of Plasticity* 56, 183–202.
- 493 Luo, T., Gao, X., 2018. On the prediction of ductile fracture by void coalescence and strain
494 localization. *Journal of the Mechanics and Physics of Solids* 113, 82–104.
- 495 Marciniak, Z., Kuczyński, K., 1967. Limit strains in the processes of stretch-forming sheet metal.
496 *International Journal of Mechanical Sciences* 9, 609–620.
- 497 Marciniak, Z., Kuczyński, K., Pokora, T., 1973. Influence of the plastic properties of a material
498 on the forming limit diagram for sheet metal in tension. *International Journal of Mechanical*
499 *Sciences* 15, 789–800.
- 500 Mear, M., Hutchinson, J., 1985. Influence of yield surface curvature on flow localization in dilatant
501 plasticity. *Mechanics of Materials* 4, 395–407.
- 502 Mercier, S., Molinari, A., 2003. Predictions of bifurcations and instabilities during dynamic ex-
503 tensions. *International Journal of Solids and Structures* 40, 1995–2016.
- 504 Nahshon, K., Hutchinson, J., 2008. Modification of the guron model for shear failure. *European*
505 *Journal of Mechanics A-Solid* 27, 1–17.
- 506 Needleman, A., Rice, J., 1978. Limits to ductility set by plastic flow localization. in: D.P. Koistinen
507 et al., eds., *Mechanics of Sheet Metal Forming*, Plenum Publishing, New York, 237–367.
- 508 Nemat-Nasser, S., Iwakuma, T., Accorsi, M., 1986. Cavity growth and grain boundary sliding in
509 polycrystalline solids. *Mechanics of Materials* 5, 137–144.

- 510 Ortiz, M., Molinari, A., 1992. Effect of strain hardening and rate sensitivity on the dynamic
511 growth of a void in a plastic material. *Journal of Applied Mechanics* 114, 48–53.
- 512 Osovski, S., Srivastava, A., Ponson, L., Bouchaud, E., Tvergaard, V., Ravi-Chandar, K., Needle-
513 man, A., 2015. The effect of loading rate on ductile fracture toughness and fracture surface
514 roughness. *Journal of the Mechanics and Physics of Solids* 76, 20–46.
- 515 Pan, J., 1983a. Perturbation analysis of shear strain localization in rate sensitive materials. *Inter-
516 national Journal of Solids and Structures* 19, 153–164.
- 517 Pan, J., Saje, M., Needleman, A., 1983. Localization of deformation in rate-sensitive porous plastic
518 solids. *International Journal of Fracture* 21, 261–278.
- 519 Pan, J. and Rice, J., 1983b. Rate sensitivity of plastic flow and implications for yield surface
520 vertices. *International Journal of Solids and Structures* 19, 973–987.
- 521 Pardoën, T., Hutchinson, J., 2000. An extended model for void growth and coalescence. *Journal
522 of the Mechanics and Physics of Solids* 48, 2467–2512.
- 523 Pineau, A., Benzerga, A., Pardoën, T., 2016. Failure of metals i: Brittle and ductile fracture. *Acta
524 Materialia* 107, 424–483.
- 525 Rice, J., 1977. The localization of plastic deformation. In: Koiter, W.T., (Ed.), *Theoretical and
526 Applied Mechanics*, North-Holland, 207–220.
- 527 Rudnicki, J., Rice, J., 1975. Conditions for the localization of deformation in pressuresensitive
528 dilatant materials. *Journal of the Mechanics and Physics of Solids* 23, 371–394.
- 529 Saje, M., Pan, J., Needleman, A., 1982. Void nucleation effects on shear localization in porous
530 plastic solids. *International Journal of Fracture* 19, 163–182.
- 531 Scheyvaerts, F., Onck, P., Tekoğlu, C., Pardoën, T., 2011. The growth and coalescence of ellip-
532 soidal voids in plane strain under combined shear and tension. *Journal of the Mechanics and
533 Physics of Solids* 59, 373–397.
- 534 Srivastava, A., Needleman, A., 2013. Void growth versus void collapse in a creeping single crystal.
535 *Journal of the Mechanics and Physics of Solids* 61 (5), 1169–1184.
- 536 Srivastava, A., Ponson, L., Osovski, S., Bouchaud, E., Tvergaard, V., Needleman, A., 2014. Effect
537 of inclusion density on ductile fracture toughness and roughness. *Journal of the Mechanics and
538 Physics of Solids* 63, 62–79.
- 539 Taya, M., Seidel, E., 1981. Void growth in a viscous metal. *International Journal of Engineering
540 Science* 19, 1083–1094.
- 541 Tekoğlu, C., Hutchinson, J., Pardoën, T., 2015. On localization and void coalescence as a precursor
542 to ductile fracture. *Phil. Trans. R. Soc. A* 373 (2038), 20140121.

- 543 Torki, M., Tekoğlu, C., Leblond, J., Benzerga, A., 2017. Theoretical and numerical analysis of void
544 coalescence in porous ductile solids under arbitrary loadings. *International Journal of Plasticity*
545 91, 160–181.
- 546 Tvergaard, V., 1981. Influence of voids on shear band instabilities under plane strain conditions.
547 *International Journal of Fracture* 17, 389–407.
- 548 Tvergaard, V., 1982. On localization in ductile materials containing spherical voids. *International*
549 *Journal of fracture* 18 (4), 237–252.
- 550 Tvergaard, V., 1989. Numerical study of localization in a void-sheet. *International journal of solids*
551 *and structures* 25 (10), 1143–1156.
- 552 Vadillo, G., Reboul, J., Fernández-Sáez, J., 2016. A modified gurson model to account for the
553 influence of the lode parameter at high triaxialities. *European Journal of Mechanics A/Solids*
554 56, 31–44.
- 555 Vadillo, G., Rodríguez-Martínez, J., Fernández-Sáez, J., 2012. On the interplay between strain
556 rate and strain rate sensitivity on flow localization in the dynamic expansion of ductile rings.
557 *International Journal of Solids and Structures* 49, 481–491.
- 558 Wang, H., Wu, P., Kurukuri, S., Worswick, M. J., Peng, Y., Tang, D., Li, D., 2018. Strain rate
559 sensitivities of deformation mechanisms in magnesium alloys. *International Journal of Plasticity*
560 107, 207–222.
- 561 Yamamoto, H., 1978. Conditions for shear localization in the ductile fracture of void-containing
562 materials. *International Journal of Fracture* 14, 347–365.
- 563 Yoon, H., Taya, M., 1984. Prediction of the void growth at its early stage in a viscous two-phase
564 material. *International Journal of Engineering Science* 22, 1035–1040.